Eur. Phys. J. C (2022) 82:465
https://doi.org/10.1140/epjc/s10052-022-10397-8

THE EUROPEAN PHYSICAL JOURNAL C

Regular Article - Experimental Physics

Neutrino tagging: a new tool for accelerator based neutrino experiments

Mathieu Perrin-Terrin[a]

Aix Marseille Univ, CNRS/IN2P3, CPPM, Marseille, France

Received: 24 December 2021 / Accepted: 2 May 2022 / Published online: 20 May 2022

Abstract This article describes a new experimental method for accelerator based neutrino experiments called neutrino *tagging*. The method consists in exploiting the neutrino production mechanism, the $\pi^{\pm} \to \mu^{\pm}\overset{(-)}{\nu}_{\mu}$ decay, to kinematically reconstruct the neutrino properties from the decay incoming and outgoing charged particles. The reconstruction of these particles relies on the recent progress and ongoing developments in silicon particle detector technology. A detailed description of the method and achievable key performances is presented, together with its potential benefits for short and long baseline experiments. Then, a novel configuration for long baseline experiments is discussed in which a tagged beam would be employed together with mega-ton scale natural deep water Cherenkov detectors. The coarseness of this type of detectors is overcome by the precision of the tagging and, conversely, the rate limitation imposed by the tagging is outweighed by the size of the detector. These mutual benefits result in an affordable design for next generations of long baseline experiments. The physics potential of such experiments is quantified using the Protvino to KM3NeT/ORCA setup as a case study for which an unprecedented sensitivity to the leptonic CP violation could be achieved.

1 Introduction

The discovery of neutrino oscillation with atmospheric neutrinos and its confirmation with solar neutrinos have inaugurated a rich field in fundamental physics. Following these first measurements, new experiments were designed to operate with controlled neutrino sources to more precisely measure the neutrino oscillation parameters. In this context, experiments have been performed with neutrino beams with energies of $\mathcal{O}$(1–10)GeV produced at particle accelerators. This type of experiments typically requires two neutrino detectors. The first one is installed near the accelerator to characterise the initial neutrino flux. The second one is placed further downstream and measures the flux after oscillation. For studying the standard neutrino oscillation, the distance over which the neutrinos propagate has to be $\mathcal{O}$(100–1000) km. Hence, these setups are referred to as long baseline neutrino experiments (LBNE's) in contrast to short baseline neutrino experiments (SBNE's) for which the distance of propagation is $\mathcal{O}$(10–100) m. The physics case of the latter is the study of non-standard neutrino oscillations, neutrino cross-sections and interactions.

The first generations of LBNE's, K2K, MINOS, T2K, NOVA, have successfully improved the knowledge on the mixing angles and the squared mass splittings. The next generation of experiments, DUNE [1–3] and T2HK [4,5], are being constructed to determine the neutrino mass ordering and to study CP violation in the neutrino sector. These new experiments rely on the same methodology but employ larger detectors and more powerful beams to collect larger neutrino samples. Moreover, they implement new techniques such as movable near detectors to better characterise the neutrino flux and so reduce the systematic uncertainties. In parallel to these LBNE's, several SBNE's, have been carried out: LSND, MiniBooNE and MicroBooNE. These experiments have indicated anomalous oscillation patterns which, as of today, still remain puzzling.

In all these SBNE's and LBNE's, the properties of the neutrinos are obtained based solely on the neutrino interaction final state. This article proposes a new method to refine the measurement of these properties by also exploiting the neutrino production mechanism, the $\pi^{\pm} \to \mu^{\pm}\overset{(-)}{\nu}_{\mu}$ decay. The principles of the method are described in Sect. 2. In Sect. 3, a generic experimental setup using this method is presented together with estimates for the most relevant technical performances. In Sect. 4, this generic design is applied to the

ANR-19-CE31-0009.

[a] e-mail: mathieu.perrin-terrin@cppm.in2p3.fr (corresponding author)

case of a LBNE and preliminary sensitivity estimates to key observables are presented to illustrate the physics potential of the setup. Finally, summary and prospects are discussed in Sect. 5.

2 The neutrino tagging method

2.1 Conceptual description

The neutrino beams produced at accelerators are primarily obtained by generating an intense beam of pions that decay in flight as $\pi^{\pm} \to \mu^{\pm}\overset{(-)}{\nu}_{\mu}$. The possibility of extracting useful information from the decay has been identified early [6–9] but never completely implemented as proposed in this article.[1] Continuous progress in silicon pixel detectors [11–13] allows to operate beam trackers at increasingly high particle rates such that a neutrino beam line instrumented with silicon trackers becomes conceivable. These instruments would allow to reconstruct all $\pi^{\pm} \to \mu^{\pm}\overset{(-)}{\nu}_{\mu}$ decays from the tracks of the incoming $\pi^{\pm}$ and outgoing $\mu^{\pm}$. Using this information, for each decay, a *tagged* neutrino could be formed with the following properties:

- a muonic initial neutrino flavour, to match the charged lepton one,
- a chirality opposite to the lepton one, or deduced from the pion electric charge,
- a direction and energy fulfilling momentum and energy conservation at the decay.

Based on time and angular coincidence, each neutrino interacting in the detector could be associated with a single tagged neutrino. The resulting *associated* neutrino sample would allow to access to a rich physics program, as described in the next section.

2.2 Expected benefits

The neutrino *tagging* technique has three main advantages. First, it enables the reconstruction of nearly all neutrinos in the beam. Second, it allows to track each interacting neutrino from the detection back to the production at the $\pi^{\pm} \to \mu^{\pm}\overset{(-)}{\nu}_{\mu}$ decay. This ability allows in turn to precisely reconstruct the interacting neutrino properties by exploiting the decay kinematics. These advantages enter in numerous ways into the study of neutrino physics as described in the next paragraphs.

Improved flux measurement The ability to precisely and individually reconstruct all beam neutrinos from $\pi^{\pm} \to \mu^{\pm}\overset{(-)}{\nu}_{\mu}$ decays is very useful to determine the neutrino flux and its composition in terms of energy, flavour and chirality.

At SBNE's, the angular resolution on the tagged neutrinos is sufficient to perfectly determine the neutrino flux, *i.e.* predict individually which beam neutrino from $\pi^{\pm} \to \mu^{\pm}\overset{(-)}{\nu}_{\mu}$'s are in the detector acceptance. Such a perfect flux determination is extremely useful to measure neutrino cross sections.

At LBLNE's, the angular resolution might not be sufficient to predict, event-by-event, which tagged neutrinos are in the detector acceptance. However, the tagging provides stringent constraints on the ratio of the flux at the far and near detectors. This ratio is a significant source of uncertainties for oscillation studies [14,15].

Background suppression One of the main backgrounds for the studies of neutrino oscillation in the appearance $\overset{(-)}{\nu}_{\mu} \to \overset{(-)}{\nu}_{e}$ channels at SBNE and LBNE are the non-oscillated $\overset{(-)}{\nu}_{e}$ beam components [14,16,17]. The tagging technique would allow to significantly reduce this background [18] as the non-oscillated interacting $\overset{(-)}{\nu}_{e}$ will not coincide with any tagged $\overset{(-)}{\nu}_{\mu}$ and could thus be discarded.

Improved energy reconstruction The *tagged* neutrino energy measurement is expected to largely surpass the methods relying on the neutrino interaction. To illustrate this, one can consider the most forward neutrinos which are very relevant for on-axis LBNE's. These neutrinos have an energy, E_{ν}, equal to

$$E_{\nu} = (1 - m_{\mu}^2/m_{\pi}^2) \cdot E_{\pi} = 0.43 \cdot E_{\pi}, \quad (1)$$

where m_{μ} and m_{π} are the $\mu^{\pm}$ and $\pi^{\pm}$ masses and E_{π} the $\pi^{\pm}$ energy. Hence, the E_{ν} resolution is equal to the $\pi^{\pm}$ energy resolution which, in the ultrarelativitic hypothesis, is equal to the $\pi^{\pm}$ momentum resolution. A magnetic spectrometer can easily provide $\mathcal{O}(0.1-1)\%$ precision for $\pi^{\pm}$'s with momenta of $\mathcal{O}(1-10)$ GeV/c [11,19] with almost no uncertainties on the energy scale. By contrast, the reconstruction of the energy from the neutrino interaction final state is much more challenging. For instance, in a charged current (CC) interaction, the charged lepton recoils against an hadronic system which is subject to substantial stochastic fluctuations. These fluctuations induce variations of the light yield at Cherenkov water detectors [20], and of the ionisation charge at liquid argon detectors [21]. As a result, the resolutions obtained with these detectors are about one order of magnitude worse than the one expected with the tagging technique. Moreover, relating the light yield or the ionisation charge to the neutrino energy relies on interaction models which induce significant uncertainties on the energy scales. These effects are notably detrimental to the study of neutrino oscillations [22,23].

Hence, the tagging technique allows to further reduce systematic uncertainties related to energy reconstruction and opens new possibilities to resolve the energy dependent patterns of the neutrino oscillation. This ability will further help

[1] At Protvino [10], few interactions of neutrinos from $\pi^{\pm} \to \mu^{\pm}\overset{(-)}{\nu}_{\mu}$ were associated with the $\mu^{\pm}$ from the decay.

to reduce the impact of systematic uncertainties as pointed in the conclusions of [14].

Improved neutrino flavour identification The tagged neutrino energy reconstruction is independent of the neutrino interaction final state. Hence, by comparing the tagged neutrino energy to the visible energy deposited in the detector by the interacting neutrino, one could determine the process undergone by the neutrino during the interaction.

For example, this ability would allow to identify NC events as they release a smaller visible energy than CC interactions due to the outgoing neutrinos. The rate and spectrum of the NC events are unaffected by the neutrino oscillation. Hence they are conventionally considered as a background for the oscillating signal. However, in a tagged experiment, not only these events could be isolated from the signal, but they could also serve the analysis for instance to further constrain the neutrino flux.

Similarly, $\overset{(-)}{\nu}_\tau$'s undergoing CC interaction release a smaller visible energy than $\overset{(-)}{\nu}_\mu$-CC's or $\overset{(-)}{\nu}_e$-CC's due to the neutrinos produced by the $\tau^\pm$ decay. Hence, the same technique could be used to select a neutrino sample enriched in $\overset{(-)}{\nu}_\tau$. Such a sample would be extremely valuable as the $\overset{(-)}{\nu}_\tau$ appearance channel is essential to constrain the oscillation matrix unitarity [24].

Improved neutrino interaction modeling The precise flux determination and energy reconstruction provided by the tagging would allow to improve cross-section measurements, which will be very important for the next generations of LBNE's [14]. Indeed, the nearly perfect knowledge of the flux would allow to reduce the uncertainties on $\overset{(-)}{\nu}_\mu$ absolute cross sections but also the energy dependence.

Moreover, as tagged neutrinos are reconstructed independently of the neutrino interaction final state, they are excellent probes to refine the phenomenological models used to infer the neutrino energy from the neutrino–nucleus interactions [22,23].

Event by event chirality determination The tagging technique allows to determine event-by-event the neutrino chirality. Hence in a tagged neutrino experiment, the alternation of the beam polarity is no longer needed and both neutrinos and anti-neutrinos can be collected together. This ability allows to collect data samples twice as large as the ones that a conventional beam experiment would for the same beam power and data taking period. Moreover, collecting both chiralities together is a strong asset to further reduce systematic uncertainties in the attempt to precisely determine the leptonic CP violating phase for which, the asymmetry between neutrinos and anti-neutrinos is crucial.

3 Experimental setup design

The two keystones of the tagging technique are the abilities to track all charged particles in a neutrino beam line and to associate the interacting neutrinos to the tagged ones. The following paragraphs describe how these two challenges can be addressed.

3.1 Tracking capabilities

Until recently, the use of silicon pixel trackers inside a neutrino beam line was prevented by the very high particle rates of these environments. In the past few years, significant progress has been achieved to increase the particle rate at which these instruments can be operated. In particular, the NA62 Collaboration has developed a beam tracker, called GigaTracKer [11,25,26], able to withstand an instantaneous hadron rate of $750{\cdot}10^6$ particle/s with a peak flux of $2.0{\cdot}10^6$ particle/s/mm^2. The particle tracking at these rates is possible thanks to time-resolved pixels with a resolution of 130 ps. The detector life time in this environment is limited and expected to correspond to a total integrated fluence normalised, under the Non Ionizing Energy Loss (NIEL) scaling hypothesis, to a 1 MeV neutron equivalent fluence of $\mathcal{O}(10^{14-15})1$ MeV n_{eq}/cm^2. The LHC experiments have started to develop similar detectors [27,28] for the high luminosity LHC (HL-LHC) upgrade foreseen for 2028. These detectors should be able to operate at even higher particle rates. They foresee a maximum flux of $20{\cdot}10^6$ particle/s/mm^2, a total fluence of $\mathcal{O}(10^{16-17})1$ MeV n_{eq}/cm^2 and a hit time resolution of 30 ps. Assuming that the beam particles are spread over $\mathcal{O}(0.1)$ m^2, these devices would allow to track a beam with a rate of $\mathcal{O}(10^{12})$ particle/s and survive several years in such an environment. The next section describes how a neutrino beam line could be designed to keep the particle rate within the tracker capabilities.

3.2 Beam line

Three handles are available to reduce the beam particle rate. First, the particles can be spread in time by extracting them from the accelerator over a few seconds instead of the few micro-seconds cycle conventionally used. Second, the particles can be spread in space by adapting the beam transverse profile. Last, the particles can be momentum selected to keep only the $\pi^\pm$'s that would produce neutrinos in an energy range relevant for the phenomena under study.

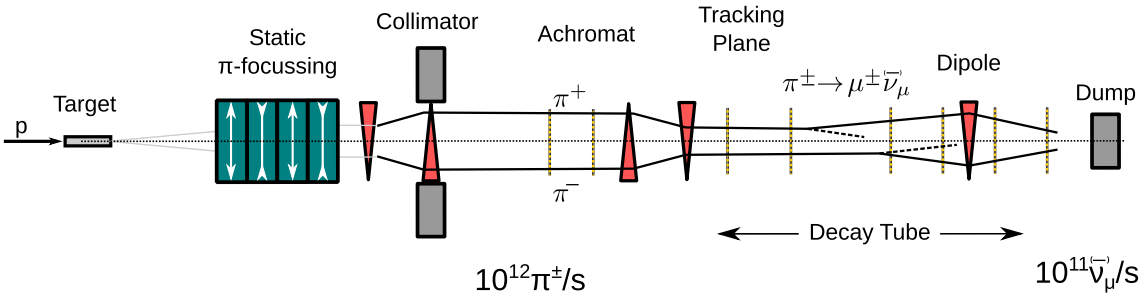

Fig. 1 Schematic of a possible beam line enabling neutrino tagging. Blue rectangles represent quadrupoles, red triangles dipoles and vertical dotted lines correspond to tracking planes. The number and location of those are not optimised. The schematic is described in more details in the text

While reducing the $\pi^\pm$ rate, the slow extraction is also preventing the use of magnetic pulsed horns traditionally employed to collimate the $\pi^\pm$'s. These elements could be replaced with quadrupoles [29]. The ENUBET collaboration has recently demonstrated that quadrupoles sets [30] can effectively reach a focusing power comparable to those of horns. Moreover, the quadrupoles can be arranged to focus both π^+ and π^-. While this feature is considered to be problematic for conventional beams, it is clearly desired for a tagged beam where the neutrino chirality is determined event-by-event.

Based on these considerations, a beam line design, as shown in Fig. 1, could be envisaged. In this design, the protons are brought onto the target over few seconds using a slow extraction. The charged particles emerging from the target are refocused using four quadrupoles to ensure similar acceptances for π^+'s and π^-'s. Then, the particles are momentum-selected by a dipole magnet and a collimator. This momentum selection is expected to reduce the particle rate by one to two orders of magnitude by removing the low momentum charged particles [31]. The beam is split into two branches by the dipole. The positively charged particles are deflected in one direction and the negatively charged one in the opposite direction. In each branch, the beam particles are restored on trajectories parallel to the initial ones by a dipole magnet with magnetic field opposite to the first one. Finally, the same arrangement of magnets, but placed in reversed order, restore the beam particles on trajectories aligned with the initial ones. The four magnets are thus forming an achromat. Two sets of time-resolved tracking stations are installed inside and after the achromat. They allow to measure the direction of the $\pi^\pm$ as the particle trajectories inside and outside the achromat are parallel. The momentum is obtained by measuring the displacement between the two trajectories which scales with the particle rigidity. The $\pi^\pm$'s then traverse a $\mathcal{O}(100)$ m long beam pipe where they may decay. At the end of the decay pipe, a dipole magnet with two sets of tracking stations, one after and one before the magnet, allow to measure the $\mu^\pm$ direction, electric charge and momentum.

The beam line section upstream of the decay tube entrance has to be as short as possible as $\pi^\pm \to \mu^\pm \overset{(-)}{\nu}_\mu$ decays occurring in this place cannot be reconstructed. Fortunately, the amount of neutrinos from early decays that happen to be in the far detector acceptance are significantly reduced by the improper collimation of the $\pi^\pm$ beam up to the last quadrupole. Likewise, after the last dipole magnet and tracking plane, the particles should be stopped as quickly as possible to prevent untrackable $\pi^\pm$ and $\mu^\pm$ decays.

The $\pi^\pm$ rates shown in Fig. 1 are derived assuming the capabilities of the HL-LHC trackers and a beam transverse size of at least 0.1 m^2. The neutrino rate is derived from this value assuming that the $\pi^\pm$ momentum is $\mathcal{O}$(1–10) GeV/c and the beam pipe is $\mathcal{O}(100)$ m long.

3.3 Interacting and *Tagged* neutrinos association

The tagging technique relies on the unambiguous matching between the interacting neutrino and tagged neutrino. This matching is performed based on time and angular coincidences.

The tagged neutrino time coordinate will be determined with great precision, as each pixel layer will provide an independent time measurement with $\mathcal{O}(10)$ ps resolution. Hence the size of the matching time window will be determined, in the first place, by the resolution on the interacting neutrino. The latter is typically $\mathcal{O}(10)$ ns. Given this value and a neutrino flux of 10^{11} ν/s, about $\mathcal{O}(10^3)$ tagged neutrinos will coincide in time with a given interacting neutrino.

The number of accidentally matching tagged neutrinos will further be reduced by using the angular coincidence between them and the interacting neutrino. The efficiency to reduce the number of matches is determined by the resolutions on the tagged and interacting neutrinos' directions.

The direction of the interacting neutrino can be derived as the ratio of the transverse position of the neutrino interaction to the baseline. The resolution on the interaction position depends on the technology used for the neutrino detector and ranges from meters, for the sparsest instruments [32], to millimeters for the densest ones [1,33]. Using the most spatially

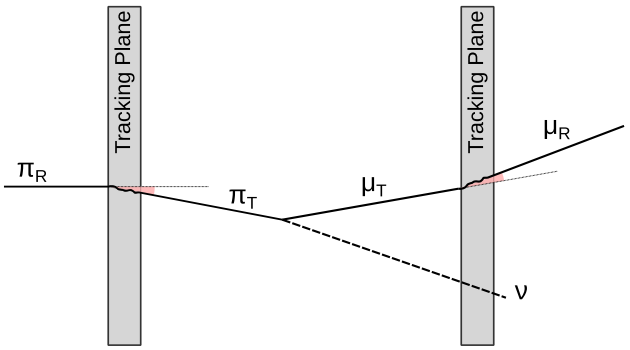

Fig. 2 Schematic describing the hypothesis made on the achievable resolutions on $\pi^{\pm}$ and $\mu^{\pm}$ direction. At the decay point, the reconstructed $\pi^{\pm}$ and $\mu^{\pm}$ directions, π_R and μ_R, differ from the true ones, π_T and μ_T, as the $\pi^{\pm}$ and $\mu^{\pm}$ undergo multiple coulomb scattering in the last and first tracking plane they respectively cross

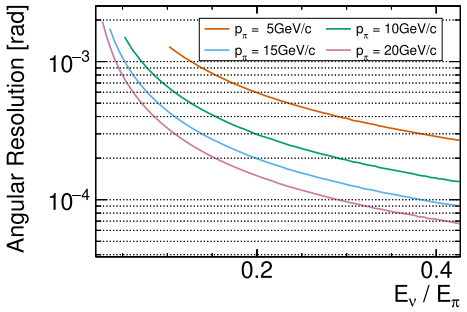

Fig. 3 Angular resolution on the tagged neutrino as a function of the fraction of the $\pi^{\pm}$ energy transferred to the neutrino for different $\pi^{\pm}$ momenta

resolved detectors technology for SBNE's, and coarser ones for LBNE's, one can always achieve angular resolutions better than $\mathcal{O}(10)$ μrad.

The angular resolution on the tagged neutrino is determined by the performances of the beam spectrometers. In this study, these performances are assumed to be similar to the ones of the existing NA62 GigaTracKer [11]. The momentum resolution is 0.2% for the $\pi^{\pm}$ and $\mu^{\pm}$. The resolution on the $\pi^{\pm}$ and $\mu^{\pm}$ direction is limited by the multiple coulomb scattering that the $\pi^{\pm}$ and $\mu^{\pm}$ undergo, respectively, in the last and first tracking plane they crossed, as illustrated in Fig. 2. The tracking planes are assumed to have a thickness of 0.5% of a radiation length as for the NA62-GigaTraKer [11].

Under these hypotheses, the standard deviation on the space angle between the true and the reconstructed neutrino is shown in Fig. 3 for different incoming $\pi^{\pm}$ momenta and as a function of the neutrino energy.[2]

The best resolutions are achieved for high momentum $\pi^{\pm}$'s and high energy $\overset{\leftrightarrow}{\nu}_{\mu}$'s which are emitted colinear to the $\pi^{\pm}$'s. On average, the tagged neutrino angular resolution ranges between 0.1 and 1 mrad. These values are one to two orders of magnitude worse than the angular resolutions obtained for the interacting neutrinos. Hence, the capability to correctly associate tagged and interacting neutrinos, based on the angular coincidence, is determined in the first place by the tagged neutrino resolution.

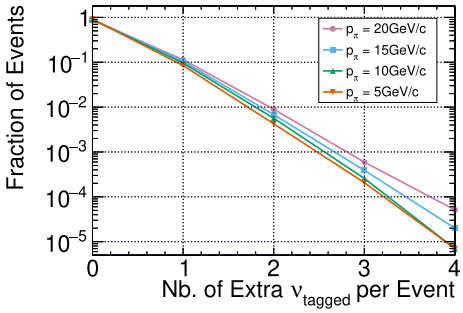

Fig. 4 Distribution of the number of extra tagged neutrinos in coincidence with the interacting neutrinos assuming different $\pi^{\pm}$ momenta

This resolution has to be compared with the tagged neutrino angular distribution. The wider this distribution, the smaller the number of accidentally matching tagged neutrinos. Hence, a conservative hypothesis consists in assuming that the $\pi^{\pm}$ beam is perfectly focused and that the $\overset{\leftrightarrow}{\nu}_{\mu}$ beam divergence arises only from the $\pi^{\pm} \rightarrow \mu^{\pm}\overset{\leftrightarrow}{\nu}_{\mu}$ decay. In these conditions, the $\overset{\leftrightarrow}{\nu}_{\mu}$ beam divergence is around $1/\gamma$, where γ is the $\pi^{\pm}$ Lorentz boost. For $\pi^{\pm}$'s with a momentum of 15 GeV/c, the beam divergence is $\mathcal{O}(10)$ mrad while the angular resolution is about $\mathcal{O}(0.1)$ mrad. As a result, the number of accidentally matching tagged neutrinos will be reduced by a factor $(0.1/10)^2$, going from 1000 to 0.1. As the worsening of the resolution at lower $\pi^{\pm}$ momenta is compensated by the increase of the beam divergence, the previous result is expected to be independent of the $\pi^{\pm}$ momentum. Assuming that the number of accidentally matching tagged neutrinos follows a Poisson distribution,[3] the association between interacting and tagged neutrino will be unambiguous for 90% of the events.

More quantitative simulations have confirmed these qualitative results, as reported in Fig. 4. According to the study, tagged and interacting neutrinos can be associated without ambiguity for more than 90% of the events with a very marginal dependence on the $\pi^{\pm}$ momentum. The remaining 10% of the events would have to be discarded for physics analyses as the association is ambiguous. Background from mis-associated events would only occur if the true tagged neutrino is not reconstructed. Such a situation occurs when the $\pi^{\pm}$'s decay before the trackers. These early decays represent the main source of missing tagged neutrinos. Com-

[2] As a reminder, the neutrino energy is uniformly distributed between $E_\nu/E_\pi = 0$ and 0.43.

[3] This hypothesis may be optimistic as time structures in the beam may remain due to improper de-bunching.

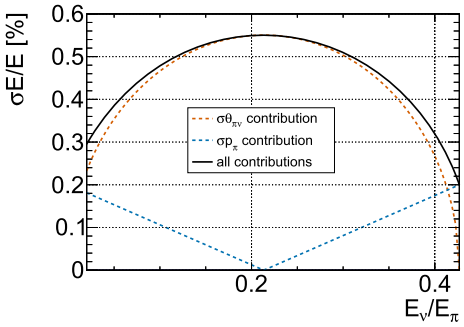

Fig. 5 Energy resolution on the tagged neutrino as a function of the fraction of the $\pi^{\pm}$ energy transferred to the ν (black solid) overlaid with the contributions from the resolutions on the angle between the $\pi^{\pm}$ and ν (red dashed) and on the $\pi^{\pm}$ momentum (blue dashed)

pared to it, other sources, like tracking inefficiencies, can be made negligible. Assuming that the fraction of interacting neutrinos originating from early decays is of the order of $\mathcal{O}(1)\%$, the probability for a mis-tagged event is thus $\mathcal{O}(0.1)\%$. Hence, these results, obtained with conservative hypotheses, indicate that neutrino tagging in a beam with a rate of 10^{11} $\overset{(-)}{\nu}_{\mu}$/s should be feasible with the technologies developed for the HL-LHC.

3.4 Energy resolution

As mentioned in Sect. 2.2, the neutrino energy resolution obtained from the kinematical reconstruction is expected to greatly surpass the ones obtained from neutrino detectors in the GeV energy range. The neutrino energy, E_{ν}, can be derived from the $\pi^{\pm}$ momentum, p_{π} and the angle between the $\pi^{\pm}$ and $\overset{(-)}{\nu}_{\mu}$, $\theta_{\pi\nu}$ as

$$E_{\nu} = \frac{(1 - m_{\mu}^2/m_{\pi}^2)p_{\pi}}{1 + \gamma^2\theta_{\pi\nu}^2}, \tag{2}$$

where γ is the $\pi^{\pm}$ Lorentz boost.

The uncertainties on neutrino direction can be assumed to be negligible (see Sect. 3.3). Hence the uncertainty on $\theta_{\pi\nu}$ is dominated by the multiple coulomb scattering of the $\pi^{\pm}$ in the last tracking plane it crossed. Assuming a momentum resolution on the $\pi^{\pm}$ similar to what is achieved at NA62 [11,26] ($\sigma_p/p = 0.2\%$), the neutrino energy resolution is expected to range between 0.6% and 0.2% as shown in Fig. 5, and is independent of the $\pi^{\pm}$ momentum.

3.5 Prospects for an experimental demonstrator

In the short term, the NA62 experiment should be able to demonstrate the feasibility of the neutrino tagging technique. The collaboration is aiming at collecting about 10^{13} 75 GeV/c kaon decays [25,26] and most of them are $K^+ \to \mu^+\nu_{\mu}$. Given the size of the NA62 liquid krypton calorimeter (20 ton) [34], few hundreds of ν_{μ} should interact in the krypton. These events could then be matched with the K^+ and μ^+ reconstructed in the NA62 spectrometers. Since 2021, a trigger line dedicated to these events has been operational.

4 *Tagged* long baseline neutrino experiments

4.1 A new paradigm

The next generation of LBNE's will be devoted to the precision measurement of the neutrino oscillation parameters and in particular the CP violating phase δ_{CP}. These measurements require both large neutrino samples and small systematic uncertainties. In this context, the tagging technique would be very advantagous as it would greatly reduce the systematic uncertainties as explained in Sect. 2.2.

However, the limitation imposed by the tagging on the beam particle rate prevents to use this method for the new generation of experiments, DUNE [1–3] and T2HK [4,5], as they are relying on beams of very high intensity to collect enough statistics.

A tagged LBNE would thus need a very large detector to collect enough neutrinos with a modest beam intensity. An interesting option is to use natural water Cherenkov neutrino detectors such as KM3NeT/ORCA [32]. Compared to most of the neutrino telescopes like ANTARES [35], KM3NeT/ARCA [32], IceCube [36] or Baikal-GVD [37], which are primarily dedicated to neutrinos with energy above 1 TeV, KM3NeT/ORCA specifically aims at studying the oscillations of atmospheric neutrinos in the energy range between 3 and 100 GeV. Using this technology, very large volumes of water can be instrumented for reasonable costs, as no excavation is required. For example KM3NeT/ORCA will instrument around 6.8 Mton of sea water, i.e. a number of scattering centres more than a hundred time larger than the ones of DUNE [1–3] or HK [4,5].

While being less granular and precise than these two detectors, this technology should be sufficient for a tagged LBNE. Indeed, the initial properties of each neutrino being measured with an unprecedented precision, the detector is mainly left with the identification of the flavour of the oscillated neutrinos.

Hence, a LBNE with a tagged beam and a mega-ton scale natural water neutrino detector should provide in about ten years of operation a sample of $\mathcal{O}(10^5)$ neutrinos [38] of the highest quality with very small systematic uncertainties. This option is therefore a viable solution for the next generations of LBNE's. In the next sections a case study of such an experiment from the U70 accelerator complex in Protvino, Russia, to KM3NeT/ORCA is presented. Note that similar LBNE's could be implemented between U70 and lake Baikal in Russia

or between Fermilab and the Neptune submarine infrastructure offshore of British Columbia [39].

4.2 A tagged LBNE from Protvino to KM3NeT/ORCA

The KM3NeT/ORCA detector is under construction offshore Toulon, France and the first detection lines deployed already allowed to observe the oscillation of atmospheric neutrinos [40]. The possibility to perform a LBNE from the U70 accelerator complex in Protvino, Russia, to KM3NeT/ORCA was discussed in detail in [38]. The experiment is referred to as P2O. The baseline of 2595 km corresponds to an energy at the first oscillation maximum of around 5 GeV, as shown in Fig. 6, which is well above the detection threshold of KM3NeT/ORCA. In the following paragraphs, a study of the sensitivity to δ_{CP} of P2O with a tagged beam is presented.

The study assumes that a 450 kW wide band beam can be delivered by U70 [43]. The neutrino rates and spectra are assumed to be identical to the ones obtained in the initial P2O study [38].[4] Such a beam would allow to collect about $20 \cdot 10^3$ neutrinos and $5 \cdot 10^3$ anti-neutrinos per year with KM3NeT/ORCA. The beam power corresponds to $2.25 \cdot 10^{14}$ protons per pulse [43]. The same order of magnitude is expected for the $\pi^{\pm}$ rate after the protons interacted in the target and before any selection. This rate can be reduced by around two orders of magnitude by imposing a minimum $\pi^{\pm}$ momentum of 9 GeV/c [31]. As the maximum neutrino energy from $\pi^{\pm} \rightarrow \mu^{\pm}\overset{(-)}{\nu}_{\mu}$ is $0.43 \cdot E_{\pi}$, this selection has no effect on the neutrino with an energy around and above 5 GeV, the first oscillation maximum. The expected $\pi^{\pm}$ rate should thus be around 10^{12} particle/s which is within the capabilities of the trackers as discussed in Sect. 3.1.

For what concerns the association between interacting and tagged neutrinos, the resolution on the interacting neutrino time-of-flight will be dominated by the uncertainties on the interaction position. The later is expected to be 1 m [32] corresponding to about 3 ns which is better than the value assumed in Sect. 3.3. The individual association of the interacting neutrino with the tagged one can thus be taken as granted.

4.3 Measurement principle

The tagged P2O experimental setup will access an unprecedented neutrino energy resolution which opens new possibilities. The standard method to determine δ_{CP} [44] consists in measuring the probabilities for neutrino and anti-neutrino oscillation, $P(\nu_{\mu} \rightarrow \nu_e)$ and $P(\bar{\nu}_{\mu} \rightarrow \bar{\nu}_e)$, and in comparing them to the expectations. The latters describe two ellipses, one for each mass ordering, in the $P(\nu_{\mu} \rightarrow \nu_e) \times P(\bar{\nu}_{\mu} \rightarrow \bar{\nu}_e)$ plane. At tagged P2O, the excellent energy resolution allows to extend the method and to measure the two probabilities for different energies. Figure 7 shows these two probabilities as function of δ_{CP} and for various energies between 4 and 15 GeV. The probabilities are nearly symmetric with respect to the $P(\nu_{\mu} \rightarrow \nu_e) = P(\bar{\nu}_{\mu} \rightarrow \bar{\nu}_e)$ line. The top part corresponds to inverted ordering (IO) and the bottom to normal ordering (NO). With such a long baseline, the two orderings are well separated. Fig. 7(b) shows a zoom into the NO region. For each energy, the points corresponding to the different δ_{CP} values describe an ellipse. The points corresponding to the same δ_{CP} value follow, as the energy is varied, one of the curved lines in shades of blue. At high energy (dark red ellipses), both probabilities are null, as the oscillation is no longer occurring. Near the first oscillation maximum energy, 5 GeV, the curvature of the ellipse is maximal at $\delta_{CP} = 90°$ and 180° which translates in the well known result that the precision to measure δ_{CP} is the worse at these values. However, the ellipses apsides correspond to other δ_{CP} values for other energies. In addition, at these energies the ellipses are more circular. The excellent energy reconstruction offered by the tagging technique makes it possible to resolve the different ellipses. Hence, the degradation of the δ_{CP} precision at 90° and 180° is expected to be much less pronounced at a tagged P2O.

4.4 Detector responses

The performances of the KM3NeT/ORCA detector in terms of energy response, effective mass and particle identification (PID) are assumed to be identical to the ones obtained on atmospheric neutrinos. A detailed description of the performances is available in [45]. This hypothesis is conservative as new reconstruction and triggering algorithms could be developed to exploit the fact that the direction and energy of the beam neutrinos are known *a-priori*. A second scenario is also considered in the study where the detector photo-cathode density is assumed to be twice as large as the KM3NeT/ORCA nominal value. In this case, the performances for a given energy are assumed to be equal to those obtained at KM3NeT/ORCA for twice the energy. A third limit case scenario is also envisaged where the PID is assumed to be perfect. The energy resolution on the tagged neutrino is assumed to be 1% which is also a conservative hypothesis.

4.5 *Tagged* P2O sensitivity to δ_{CP}

With the assumptions described above, the sensitivity of tagged P2O to δ_{CP} is derived with a method similar to the one described in [45, Sect. 3.1] and using the oscillation parameters from [42]. The analysis is performed using the

[4] Studies should be performed to refine the hypotheses made on the neutrino rates and spectra as the performances of a tagged beam line can significantly differs from the ones in [32]

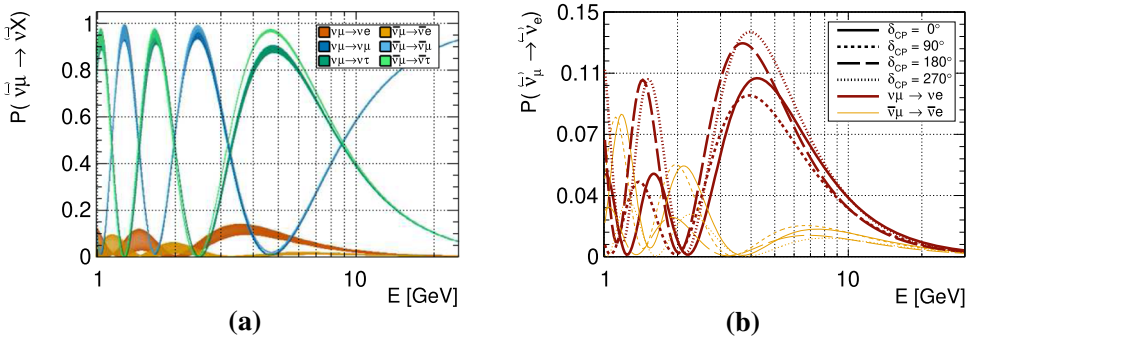

Fig. 6 **a** Probabilities for ν_μ's (dark colour scatter plots) and $\bar{\nu}_\mu$'s (light colour scatter plots) to oscillate to each neutrino flavours as function of the neutrino energy and for all possible values of δ_{CP}. **b** Probabilities for a ν_μ's (dark red thick lines) and $\bar{\nu}_\mu$'s (yellow thin lines) to oscillate to the electron neutrino flavour as a function of the neutrino energy. The probabilities for different δ_{CP} values are shown with different line styles. In both **a** and **b**, the oscillation baseline is 2595 km. The oscillation probabilities are computed with the OscProb software package [41] and using the oscillation parameters from [42]

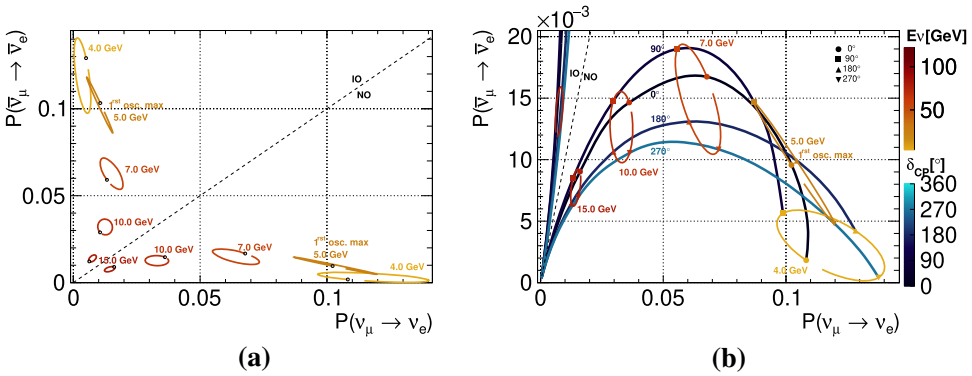

Fig. 7 **a** Probability for $\bar{\nu}_\mu$ to oscillate to $\bar{\nu}_e$ versus the probability for ν_μ to oscillate to ν_e. For each neutrino energy, the two probabilities describe an ellipse as δ_{CP} is varied. The black circles indicates the points for which δ_{CP} equals 0°. The color of the ellipses corresponds to the neutrino energy and is reported on the red color scale in **b**. The ellipses obtained assuming normal ordering (NO) and inverted ordering (IO) are clearly separated with IO above the $P(\nu_\mu \to \nu_e) = P(\bar{\nu}_\mu \to \bar{\nu}_e)$ line (dashed line) and NO below. A zoom in the NO region is shown in **b**. The blue lines represents the probabilities for a given δ_{CP} value when the energy is varied. At high energy both probabilities are null as no oscillation occurs. In both **a** and **b**, the oscillation baseline is 2595 km. The probabilities are computed with the OscProb software package [41] and using the oscillation parameters from [42]

OscProb [41] and ROOT [46] software packages. The neutrino and anti-neutrino data samples are analysed in the plane made by the energy reconstructed by the tagger and the one reconstructed by the KM3NeT/ORCA detector. Three event categories are considered based on the detector PID response: a track-like class collecting mostly $\overset{(-)}{\nu}_\mu$-CC and $\overset{(-)}{\nu}_\tau$-CC where the $\tau^\pm$ decay to a $\mu^\pm$; a shower-like class collecting mostly $\overset{(-)}{\nu}_e$-CC, NC and $\overset{(-)}{\nu}_\tau$-CC where the $\tau^\pm$ decay hadronically; and an intermediate class collecting an admixture of flavours. A full description of the KM3NeT/ORCA PID performances is available in [45, Fig. 6]. When a perfect PID is considered, four event categories are used, one for each flavour and one for the NC interaction. In this case, the analysis is performed in one dimension corresponding to the tagged neutrino reconstructed energy. The distributions of the energy reconstructed by KM3NeT/ORCA and by the tagger in each PID category is obtained by applying the detector response to the true energy distributions.

Several systematic uncertainties, reported in Table 1 are included in the model to reflect the limited knowledge on:

- the oscillation parameters, θ_{13}, θ_{23} and Δm^2_{23},
- the detector performances in terms of detection efficiency, energy scale and PID,
- the beam neutrino rates,
- the cross-section.

The choice and treatment of these uncertainties are similar to what is described in [38] and in [45, Sect. 3.1]. Technically, the systematic uncertainties are implemented with a set of energy scales and re-normalisation factors which distort the expected event distributions.

Table 1 Parameters considered as systematic uncertainties together with the standard deviation of the Gaussian priors applied to them

Parameter	Gaussian Prior Std Dev
θ_{13}	0.15°
θ_{23}	2.0°
Δm^2_{23}	$5{\cdot}10^{-3}$ eV^2
Global energy scale	3%
Hadronic energy scale	3%
$\overset{(-)}{\nu}_{e,\mu}$ energy scale	3%
PID category energy scales	3%
PID category normalisations	10%
$\overset{(-)}{\nu}_{\tau}$-CC cross section	10%
$\overset{(-)}{\nu}_{e,\mu}$ cross section	10%
NC cross section	5%

A first energy scale, referred to as *global energy scale* in Table 1, is applied to neutrinos from all channels ($\overset{(-)}{\nu}_e$, $\overset{(-)}{\nu}_\mu$ and $\overset{(-)}{\nu}_\tau$ both CC and NC) and represents the uncertainties on the detector energy response which originate from the limited knowledge on the photo-detection efficiency. The large fluctuations of the hadronic showers light yield further increase the uncertainties on the detection efficiency. Hence, a second scaling factor, referred to as *hadronic energy scale* in Table 1, is applied to neutrinos from all channels but weighted by the average fraction of light produced by the hadronic shower in the interaction. Finally, as the energy thresholds and the energy responses may differ between the channels, a third factor, referred to as $\overset{(-)}{\nu}_{e,\mu}$ *energy scale* in Table 1, is applied only to $\overset{(-)}{\nu}_{e,\mu}$-CC, as in [38].

The uncertainties on the PID response are implemented with a set of independent energy scale factors, referred to as *PID category energy scales* in Table 1, and applied to the neutrinos in each PID category. In addition, the event yields classified in each PID category are scaled by independent re-normalisation factors, referred to as *PID category normalisations* in Table 1. These re-normalisation factors reflect also the uncertainties on the total event yield which originate from the limited knowledge on the detection efficiency, beam rate and cross-sections.

As the cross sections for NC and $\overset{(-)}{\nu}_\tau$-CC interactions are less precisely known than the others, two independent re-normalisation factors, *NC cross section* and $\overset{(-)}{\nu}_\tau$*-CC cross section* in Table 1, are respectively applied to the event yields from NC and $\overset{(-)}{\nu}_\tau$-CC.

Gaussian priors are applied to these parameters. The standard deviations of these priors are identical to [38] and reported in Table 1.

The sensitivity to exclude the CP-conservation hypothesis is reported in Fig. 8 for different scenarios: standard P2O, tagged P2O and tagged P2O with a denser detector,

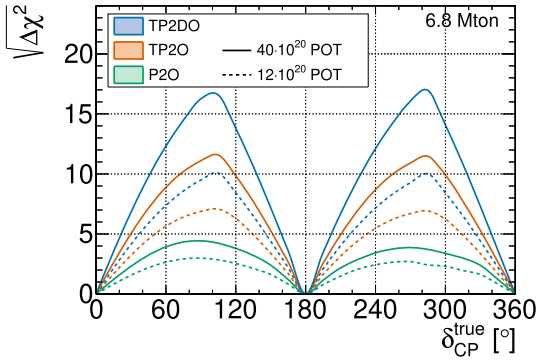

Fig. 8 Sensitivity to exclude the no-CP violation hypothesis as a function of the true δ_{CP} value for P2O (green), tagged P2O (red) and tagged P2O with a far detector with a photocathode density twice as large as KM3NeT/ORCA (blue). The solid lines correspond to an exposure of $40{\cdot}10^{20}$ POT and the dashed ones to $12{\cdot}10^{20}$ POT

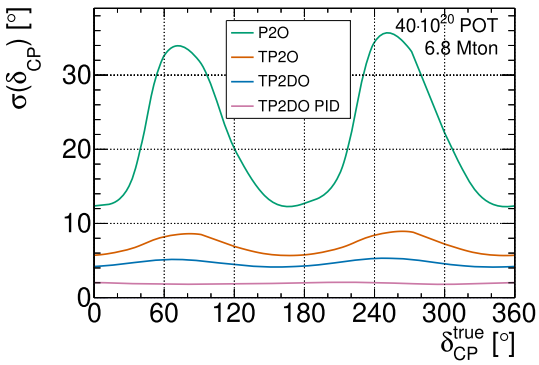

Fig. 9 Precision on δ_{CP} as a function of the true δ_{CP} value for P2O (green), tagged P2O (red), tagged P2O with a far detector with a photocathode density twice as large as KM3NeT/ORCA (blue), and with a perfect PID (purple)

and, for two different exposures: $12{\cdot}10^{20}$ protons-on-target (POT) and $40{\cdot}10^{20}$ POT corresponding to 3 and 10 years of operation with a 450 kW beam. Discovering the CP violation in the neutrino sector appears to be impossible at P2O. However such a discovery becomes possible with the tagging technique. With $12{\cdot}10^{20}$ POT, tagged P2O would be able to claim a 5σ discovery of this effect for 46% of the δ_{CP} phases violating the CP symmetry and 68% with $40{\cdot}10^{20}$ POT. These values are increased to 60% and 76% if a denser detector is used.

The precision on δ_{CP} is reported in Fig. 9 for four scenarios: standard P2O, tagged P2O, tagged P2O with a denser detector and, finally, with a perfect PID. The benefit of the tagging method is very clear. It allows to reach a much better precision and the precision obtained remains stable over the whole δ_{CP} range. In the case of tagged P2O with a dense detector, a precision between 4° and 5° is expected for an exposure of $40{\cdot}10^{20}$ POT and a water instrumented mass of 6.8 Mton. In the limit case for which a perfect PID is achieved, a 2° precision could be reached.

5 Conclusions and prospects

In this article, a new experimental method was presented for accelerator based neutrino experiments: the neutrino tagging. The method consists in exploiting the neutrino production mechanism, the $\pi^{\pm} \rightarrow \mu^{\pm}\overset{(-)}{\nu}_{\mu}$ decay, to kinematically reconstruct the neutrino properties based on the incoming and outgoing decay charged particles. The reconstruction of these particles relies on the recent progress and on-going developments in silicon particle detector technology which can operate at very high particle flux. The tagging method allows to reconstruct individually nearly all neutrinos in the beam and to determine the particle properties with an unprecedented precision. Using time and angular coincidences, the neutrino interacting in the detector can be individually matched to the $\pi^{\pm} \rightarrow \mu^{\pm}\overset{(-)}{\nu}_{\mu}$ decay it originated from and to the corresponding tagged neutrino.

The benefits brought by this method are numerous. Such a precise knowledge of the neutrino source allows to drastically reduce the systematic uncertainties and background contaminations for neutrino oscillation studies. These studies also benefit from the excellent energy resolution which allows to fully exploit the energy dependence of the oscillation probabilities. Finally, the tagging technique enables significant improvements of the cross-section measurements and of the phenomenological models used to infer the neutrino energy from the neutrino-nucleus interactions.

The implementation of this technique requires to design neutrino beam lines where the particle flux remains within the capabilities of the silicon detector technologies. Ideas were presented on how to design such a beam line using slow extraction, large beam transverse size and careful momentum selection of secondary pions. The resulting beam line layout employs only basic and affordable elements such as dipoles and quadrupoles. The beam line can simultaneously collect neutrinos and anti-neutrinos by exploiting the event-by-event chirality determination provided by the tagging. A generic beam line design is under investigation within the CERN Physics Beyond Colliders Study Group [47] and in collaboration with the Institute for High Energy Physics in Protvino. The outcome of these studies will allow to refine the hypotheses made in this article.

Based on these ideas, a new type of long baseline neutrino experiments was proposed which uses a tagged beam together with a mega-ton scale natural water Cherenkov neutrino detector. The strength of the design stems from the counterbalancing of the detector limitations by the assets of the tagging and vice-versa. Indeed, the coarseness of the sparse water Cherenkov detector is overcome by the excellent precision of the tagging and, conversely, the rate limitation imposed by the tagging is outweighed by the size of the detector.

The physics potential for this new type of long baseline experiments was evaluated with the Protvino to KM3NeT/ORCA (P2O) setup as a benchmark. The reduced systematic uncertainties and the sub-percent energy resolution yields unprecedented sensitivities to the CP violating phase δ_{CP}. Several scenarios were considered for the far detector performances extrapolating from the ones obtained with atmospheric neutrinos. These scenarios still require to be consolidated with precise studies of the KM3NeT/ORCA detector performances with tagged beam neutrinos. The most optimistic scenarios indicate that a 2° precision on δ_{CP} could be achieved. Hence, the tagging technique represents a valuable option for the next generations of neutrino experiments. More investigations will be carried out to study the complete physics case of the method at short and long baseline experiments.

Acknowledgements The study presented in this article was done under the auspices of the Centre de Physique des Particules de Marseille and the Agence Nationale de la Recherche through the ANR-19-CE31-0009 grant. The author is grateful to V. Dabhi for the discussions related to tagged neutrino angular resolution, to N. Charitonidis and E. Parozzi for their insights on beam line design, to J. Brunner for his enlightening views in numerous topics related to the neutrino oscillation, to C. Vallée for his support and valuable feedback on the *tagging* idea, and to D. Dornic for reviewing the manuscript of this article. The author is also grateful to the KM3NeT Collaboration for providing information related to the KM3NeT/ORCA detector performances, to the CERN's PBC Working Group for offering a forum to discuss new ideas and for supporting their development, to the NRC Kurchatov Institutes for discussing and studying the possibility to implement a *tagged* beam between Protvino and KM3NeT/ORCA and, to the NA62 Collaboration for offering the possibility to experimentally demonstrate the feasibility of the *tagging* method.

Data Availability Statement This manuscript has no associated data or the data will not be deposited. [Authors' comment: The work presented in this article is based on simulations.]

Funded by SCOAP[3].

References

1. B. Abi et al., Eur. Phys. J. C **80**(10), 978 (2020). https://doi.org/10.1140/epjc/s10052-020-08456-z
2. B. Abi, et al., Deep underground neutrino experiment (dune), far detector technical design report, volume ii: Dune physics. Tech. rep. (2020)

3. B. Abi et al., JINST **15**(08), T08008 (2020). https://doi.org/10.1088/1748-0221/15/08/T08008
4. K. Abe, et al. Hyper-Kamiokande Design Report. https://arxiv.org/abs/1805.04163 (2018)
5. Y. Itow, PoS **ICRC2021**, 1192 (2021). https://doi.org/10.22323/1.395.1192
6. B. Pontecorvo, Lett. Nuovo Cim. **25**, 257 (1979). https://doi.org/10.1007/BF02813638
7. I.P. Nedyalkov. Single spectrometer station for neutrino tagging. http://inis.jinr.ru/sl/NTBLIB/JINR-E1-84-515.pdf (1984)
8. G. Bohm. Project of a tagged neutrino facility at serpukhov. https://inis.iaea.org/collection/NCLCollectionStore/_Public/21/060/21060898.pdf (1987)
9. R.H. Bernstein, et al. A Proposal for a Neutrino Oscillation Experiment in a Tagged Neutrino Line. https://inspirehep.net/files/94bcaf83ca2fdca7476a57e6182e4868 (1990)
10. V.B. Anikeev et al., Nucl. Instrum. Meth. A **419**, 596 (1998). https://doi.org/10.1016/S0168-9002(98)00837-7
11. G. Aglieri Rinella, et al., JINST **14**, P07010 (2019). https://doi.org/10.1088/1748-0221/14/07/P07010
12. A. Lai, (IEEE, Sydney, NSW, Australia, 2018), pp. 1–3. https://doi.org/10.1109/NSSMIC.2018.8824310
13. H.F.W. Sadrozinski et al., Nucl. Instrum. Meth. A **730**, 226 (2013). https://doi.org/10.1016/j.nima.2013.06.033
14. P. Huber et al., JHEP **03**, 021 (2008). https://doi.org/10.1088/1126-6708/2008/03/021
15. A. Branca, G. Brunetti, A. Longhin, M. Martini, F. Pupilli, F. Terranova, Symmetry **13**(9), 1625 (2021). https://doi.org/10.3390/sym13091625
16. A. Aguilar-Arevalo et al., Phys. Rev. D **64**, 112007 (2001). https://doi.org/10.1103/PhysRevD.64.112007
17. A. Aguilar-Arevalo et al., Phys. Rev. Lett. **110**, 161801 (2013). https://doi.org/10.1103/PhysRevLett.110.161801
18. L. Ludovici, P. Zucchelli. Conceptual study of an antitagged experiment searching for $\nu_\mu \rightarrow \mu_e$ oscillation. https://arxiv.org/abs/hep-ex/9701007
19. A.C. Booth et al., Phys. Rev. Accel. Beams **22**(6), 061003 (2019). https://doi.org/10.1103/PhysRevAccelBeams.22.061003
20. S. Adrián-Martínez et al., JHEP **05**, 008 (2017). https://doi.org/10.1007/JHEP05(2017)008
21. A. Friedland, S.W. Li, Phys. Rev. D **99**(3), 036009 (2019). https://doi.org/10.1103/PhysRevD.99.036009
22. A.M. Ankowski et al., Phys. Rev. D **92**(9), 091301 (2015). https://doi.org/10.1103/PhysRevD.92.091301
23. M. Khachatryan et al., Nature **599**(7886), 565 (2021). https://doi.org/10.1038/s41586-021-04046-5
24. S. Parke et al., Phys. Rev. D **93**(11), 113009 (2016). https://doi.org/10.1103/PhysRevD.93.113009
25. F. Hahn, et al., NA62: Technical Design Document. Tech. rep., CERN, Geneva (2010). https://cds.cern.ch/record/1404985
26. E. Cortina Gil, et al., JINST **12**(05), P05025 (2017). https://doi.org/10.1088/1748-0221/12/05/P05025
27. R. Aaij, et al., Expression of Interest for a Phase-II LHCb Upgrade: Opportunities in flavour physics, and beyond, in the HL-LHC era. Tech. rep. (2017). https://cds.cern.ch/record/2244311
28. M. van Beuzekom, J.P.S. Conf, Proc. **34**, 010014 (2021). https://doi.org/10.7566/JPSCP.34.010014
29. D.C. Carey et al., IEEE Trans. Nucl. Sci. **18**, 755 (1971). https://doi.org/10.1109/TNS.1971.4326174
30. M. Torti, et al., Int. J. Mod. Phys. A **35**(34n35), 2044017 (2020). https://doi.org/10.1142/S0217751X20440170
31. Z. Pavlovic, Studies of the neutrino flux for the numi beam at fnal. Ph.D. thesis, PhD Thesis, University of Texas at Austin (2008). https://lss.fnal.gov/archive/thesis/2000/fermilab-thesis-2008-59.pdf
32. S. Adrian-Martinez et al., J. Phys. **G43**(8), 084001 (2016). https://doi.org/10.1088/0954-3899/43/8/084001
33. Y. Fukuda et al., Nucl. Instrum. Meth. A **501**, 418 (2003). https://doi.org/10.1016/S0168-9002(03)00425-X
34. M. Jeitler, Nucl. Instrum. Meth. A **494**, 373 (2002). https://doi.org/10.1016/S0168-9002(02)01505-X
35. M. Ageron et al., Nucl. Instrum. Meth. A **656**, 11 (2011). https://doi.org/10.1016/j.nima.2011.06.103
36. M.G. Aartsen et al., JINST **12**(03), P03012 (2017). https://doi.org/10.1088/1748-0221/12/03/P03012
37. A.D. Avrorin et al., Bull. Russ. Acad. Sci. Phys. **83**(8), 921 (2019). https://doi.org/10.3103/S1062873819080057
38. A.V. Akindinov et al., Eur. Phys. J. C **79**(9), 758 (2019). https://doi.org/10.1140/epjc/s10052-019-7259-5
39. C. Vallee. Pacific neutrinos: Towards a high precision measurement of cp violation ? https://arxiv.org/abs/1610.08655
40. L. Nauta, et al., PoS **ICRC2021**, 1123 (2021). https://doi.org/10.22323/1.395.1123
41. J. Coelho. OscProb. https://github.com/joaoabcoelho/OscProb/
42. I. Esteban et al., JHEP **09**, 178 (2020). https://doi.org/10.1007/JHEP09(2020)178
43. The omega project. http://www.ihep.su/files/OMEGA%20LOI.pdf
44. K. Abe et al., Nature **580**(7803), 339 (2020). https://doi.org/10.1038/s41586-020-2177-0. [Erratum: Nature 583, E16 (2020)]
45. S. Aiello et al., Eur. Phys. J. C **82**(1), 26 (2022). https://doi.org/10.1140/epjc/s10052-021-09893-0
46. R. Brun, F. Rademakers, Nucl. Instrum. Meth. A **389**, 81 (1997). https://doi.org/10.1016/S0168-9002(97)00048-X
47. The physics beyond colliders study group. https://pbc.web.cern.ch/